Topic editor

Public justification (visible to the public if the article is accepted and published):
The manuscript presents a novel approach to estimating global Mean Leaf Inclination Angle (MLA) using satellite-derived vegetation indices and machine learning. Both reviewers acknowledge the improvements made in response to their initial comments, with many concerns adequately addressed. However, several key issues remain unresolved, warranting further revision. Reviewer 1 highlights the need for a clearer justification of the choice of EVI over other vegetation indices such as NDVI, particularly in light of recent research on vegetation index error propagation and saturation effects. Additionally, a more detailed explanation of the nonlinear LAI-EVI relationship and its saturation phenomenon is necessary. Reviewer 2 raises significant concerns regarding the upscaling methodology, particularly the transition from leaf-level LIA to ecosystem-scale MLA, emphasizing the need for a more rigorous discussion of assumptions and uncertainties. Furthermore, greater integration of responses into the manuscript, clarification of MODIS product versions, and a dedicated uncertainty assessment layer would strengthen the study's credibility. Given these remaining concerns, another major revision is necessary to ensure the robustness and transparency of the methodology, as well as to enhance the interpretability and applicability of the global MLA dataset.

We thank the topic editor for the recognition and professional processing. We fully understand the concerns raised by the reviewers and have carefully addressed these issues in this revision round.

Some major revisions were made in the revised version:

(1) The reasons for the choice of EVI2 and explanations of the nonlinear LAI-EVI2 relationship have been further elaborated in the main text.

(2) The full process of upscaling methodology has been reorganized rigorously to enhance clarity and its assumptions and uncertainty have been discussed.

(3) The uncertainty assessment layers have been added from the perspectives of inputs and the prediction model.

(4) The comments regarding MODIS products, NDVI, and GEDI LiDAR have been addressed.

(5) The responses to reviewers have been greatly integrated into the manuscript.

(6) The data DOI has been updated because of the data upgrade.

Anonymous Referee #2

After reviewing the authors' responses, I find that two of my original comments have been adequately addressed. However, one critical concern regarding the upscaling approach remains insufficiently addressed, and the resultant LIA at the ecosystem or grid scale is still rather confusing. Additionally, the authors' major responses are not clearly reflected or integrated into the revised manuscript. Below are my specific comments:

We thank the referee for the insightful comments which significantly improved the manuscript. We fully understand the referee's concerns and have provided detailed explanations and revisions below. In addition, the previous major responses to your comments regarding *Upscaling LIA Field Measurements* and *Coarse Resolution and Low-Signal Inputs in the Model* have been integrated into the revised manuscript (Sections 2.2.1, 2.3.1, and 2.3.2).

1). Upscaling LIA from the leaf level to the canopy or larger ecosystem scales is inherently challenging. Although the authors provide some clarification, their initial upscaling step remains overly simplistic, making it difficult to grasp what the "ecosystem-level LIA" truly represents. Traditionally, LIA at the canopy scale can be defined as the average LIA of each leaf (Eq. 1). However, because counting individual leaves (N) is often impractical, the authors employ a leaf-area-weighted approach for MLA. If I understand right, this equation can be defined by Eqs. 2 & 3.

$$MLA = \frac{\sum_i LIA_i}{N} \qquad (1)$$

$$MLA = \frac{\sum_j LIA_j * LA_j}{N * LA_{mean}} = \frac{\sum_j LIA_j * LA_j}{LAI * canopy\_size} \qquad (2)$$

$$LAI = N * LA_{mean}/canopy\_size = EVI2 * a + b \qquad (3)$$

Where MLA is mean inclination angle, j is the jth leaf, LIA is leaf inclination angle, N is number of leaves within a canopy, LA is single leaf area, LAI is the ecosystem-level standard leaf area index (m2/m2), canopy_size is the projected area onto the ground for a specific canopy; a and b are the linear coefficients between EVI2 and LAI (if the linear relationship holds true).

Eqs. (2) and (3) theoretically support the upscaling of LIA from the leaf to the canopy level, and by extension from the canopy to 30 m and from 30 m to 500 m. However, the authors used a simplified form of Eq (1) in the manuscript to upscale from 30m to 500m. It is hard to persuade me this equation is equivalent to the Eqs (2-3) mentioned above, especially given the existence of the interception of b and missing variable of leaf number.

In addition, the authors did not mention the details of upscaling from the canopy to 30m. As a result, the MLA on the 500m derived here and further used to training the model is difficult to interpret, which is apparently different from the LIA at the leaf level. I encourage the authors to more rigorously evaluate their upscaling methodology, discussing the assumptions and uncertainties introduced at each scale and from different data sources.

Thank the referee for this thorough comment. We have reorganized the upscaling process rigorously to enhance clarity.

From leaf to canopy scale, the entire canopy MLA is commonly calculated as the average of all measured leaf LIAs weighted by leaf area in the remote sensing community (Eq. R1) (Zou et al., 2014; De Wit, 1965; Yan et al., 2021). In practice, because of the difficulty in leaf area measurement, especially for a large number of leaves, the variability of leaf areas within a canopy is often ignored and the areas of all leaves are assumed similar. In this case, the canopy LIA can be simplified as the average LIA weighted by leaf number (Eq. R1) (Ryu et al., 2010; Pisek et al., 2011; Chianucci et al., 2018):

$$MLA_{canopy} = \frac{\sum_i LIA_i * LA_i}{\sum_i LA_i} = \frac{LA_{mean} * \sum_i LIA_i}{LA_{mean} * N} = \frac{\sum_i LIA_i}{N} \qquad \text{(R1)}$$

where MLA_{canopy} is the MLA at canopy scale, i is the ith leaf, LIA is leaf inclination angle, LA is single leaf area, LA_{mean} is the mean leaf area by ignoring the variation of leaf area within a canopy, N is number of leaves within a canopy.

From the canopy to 30 m scale, the canopy level MLA is regarded as equal to 30 m-MLA because for MLA measurements, the dominant species was artificially identified by investigators, and the spatial representativeness at the extent of 30 m is ensured. This practice has been used in previous studies to derive global maps for various leaf traits (specific leaf area, leaf dry matter content, leaf nitrogen and phosphorus content per dry mass, and leaf nitrogen/phosphorus ratio) from TRY leaf trait measurements, remote sensing, and climate data (Moreno-Martínez et al., 2018).

From 30 m to 500 m, the 500 m MLA was formulated as the weighted average of 30 m MLA by the leaf area of the 30 m pixel (Eq. R2), the same as that from the leaf to canopy scale. The leaf area of a 30 m pixel can be deduced from the product of leaf area index (LAI) and the ground area (not the projected area onto the ground for a specific canopy) of a 30 m pixel according to the definition of LAI (the half of green leaf area on the unit of ground area) (Eq. R2) (Fang et al., 2019).

$$MLA_{500} = \frac{\sum_j MLA_{30\_j} * LA_{30\_j}}{\sum_j LA_{30\_j}} = \frac{\sum_j MLA_{30\_j} * LAI_{30\_j} * S}{\sum_j LAI_{30\_j} * S} = \frac{\sum_j MLA_{30\_j} * LAI_{30\_j}}{\sum_j LAI_{30\_j}} \qquad \text{(R2)}$$

Where MLA_{500} and MLA_{30} represent MLA at 500 m and 30 m scales, *j* is the *j*th 30 m pixel, LA_{30_j} is the total leaf area of a 30 m pixel, LAI_{30_j} is leaf area index (m2/m2) of a 30 m pixel, *S* is the ground area of a 30 m pixel.

Assuming LAI=a*EVI2+b and b ≈ 0 (as illustrated in Fig. R1), the MLA at 500 m scale can be calculated as

$$MLA_{500} = \frac{\sum_j MLA_{30\_j} * EVI2_{30\_j}}{\sum_j EVI2_{30\_j}} \qquad \text{(R3)}$$

The linear relationship between LAI and EVI2 is an important assumption in the MLA upscaling. We have attempted to use the real MODIS LAI-EVI2 relationship (Fig. R1) from global statistics to correct the MLA upscaling procedure. 2,000 points for each biome type were randomly sampled and the LAI-EVI2 pairs with good quality per 8 days for these points were extracted. The LAI-EVI2 relationship is nearly linear and the intercept is close to 0 (Fig. R1).

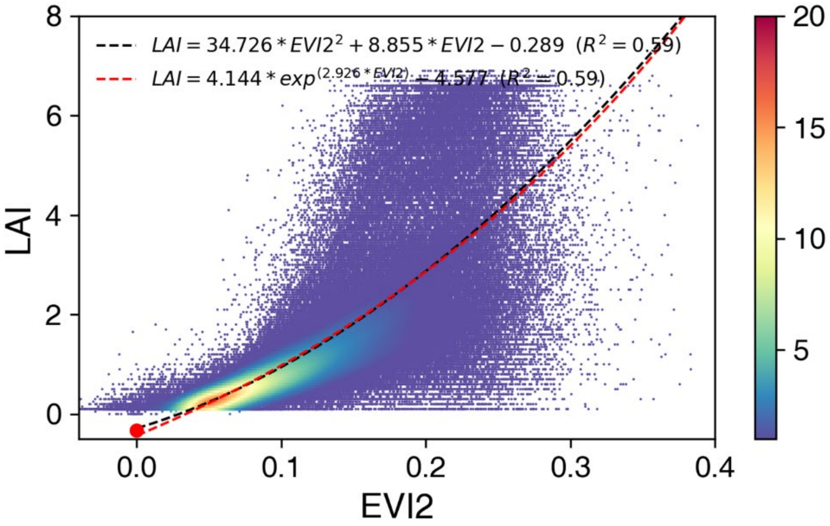

Fig. R1. The nonlinear relationship between MODIS LAI and EVI2.

Subsequently, we have updated the MLA training samples with the fitted nonlinear relationship (Fig. R1, Eq. R2) and compared the samples to the original samples based on the linear assumption (Eq. R3). The updated samples show high consistency with the original samples (Fig. R2). This may be related to the rigorous sample screening to keep the homogeneity of a 500 m sample, which reduces the impact of the LAI-EVI2 nonlinear relationship by limiting LAI variations within the 500 m pixel. Therefore, the LAI-EVI2 linear assumption is reasonable.

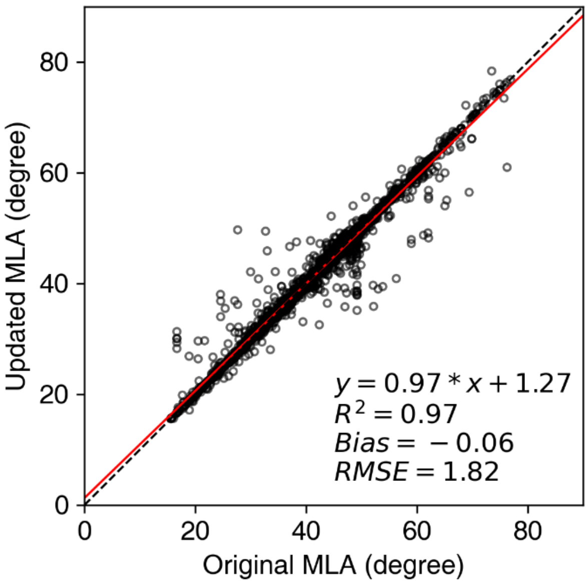

Fig. R2. The comparison between the updated samples using the LAI-EVI2 relationship and original MLA samples using EVI2. The black dashed and red solid lines represent 1:1 and fitted lines.

In addition, we agree that uncertainty may arise due to the different data sources (from TRY, literature, and manual extraction). We think the predicted MLA is robust to these differences because part of the samples and features are randomly selected in the training process and the random forest algorithm ensembles the predictions from multiple decision trees (Svetnik et al., 2003). We have manually inspected all field LIA data and are confident in their data quality.

Following the comments, we have added a detailed description regarding LIA upscaling in Appendix A and have discussed the uncertainty of the LAI-EVI2 linear relationship assumption in Section 4.4. The uncertainty raised by different data sources has been discussed in Section 4.4.

Section 4.4 LAI-EVI2 linear relationship assumption

*We assumed a linear LAI-EVI2 relationship (LAI = a*EVI2) to upscale MLA from the canopy to 500 m scale (Section 2.3.1 and Appendix A). Global analysis of MODIS LAI and EVI2 products shows a slight non-linear relationship between them (Fig. S8). The non-linear relationship was also used to upscale MLA (Eq. A2) in a side experiment, where the derived MLA was found consistent with the original one (Fig. S9) because of the homogeneity of the 500 m pixel after rigorous sample screening (section 2.3.1). This demonstrates the suitability of the linear assumption.*

Section 4.4 Different Data Sources

Second, three different sources of LIA measurements were gathered with different measurement schemes, and uncertainty may arise because of these differences. The random forest algorithm is robust to these differences because part of the samples and features were randomly selected and the algorithm ensembled the predictions from multiple decision trees (Svetnik et al., 2003). We manually inspected all field LIA data and are confident in their data quality.

2). The authors argued that “higher LIA means lower radiation interception, more NIR downward radiation, and lower NIR reflectance”, thus negatively correlated with NDVI. However, a higher LIA could also reduce red reflectance, potentially complicating how NDVI encapsulates leaf angle information. Moreover, as NDVI is designed as a normalized index, one might expect it to diminish the effects of incidence angles in BRDF data (MCD43A1). Considering the global availability of GEDI lidar (with a 25 m footprint) and its known sensitivity to canopy structure (e.g., height), it would be worthwhile to test whether GEDI can provide stronger signals of LIA than optical-only approaches. Such an investigation could bolster the validation or derivation of the first global MLA map.

We thank the referee for these comments. High LIA results in low NIR reflectance because more NIR downward radiation reaches the soil background and the NIR reflectance of soil is lower than that of vegetation (Fig. R3). In terms of red reflectance, high LIA means more red radiation penetrates the canopy and the red reflectance of soil is higher than that of vegetation because of the strong leaf absorption in this wavelength (Fig. R3), causing high red reflectance. Therefore, high LIA causes low NDVI according to its definition ((NIR-Red)/(NIR+Red)). We have rephrased the original sentence in Section 4.2:

> *Higher MLA means lower radiation interception, more NIR and red downward radiations reach the soil background. This causes lower NIR and higher red reflectance because the soil background typically has lower (higher) reflectance for NIR (red) (Siegmund and Menz, 2005). This results in negative correlations between MLA and NIR reflectance and NDVI (Liu et al., 2012).*

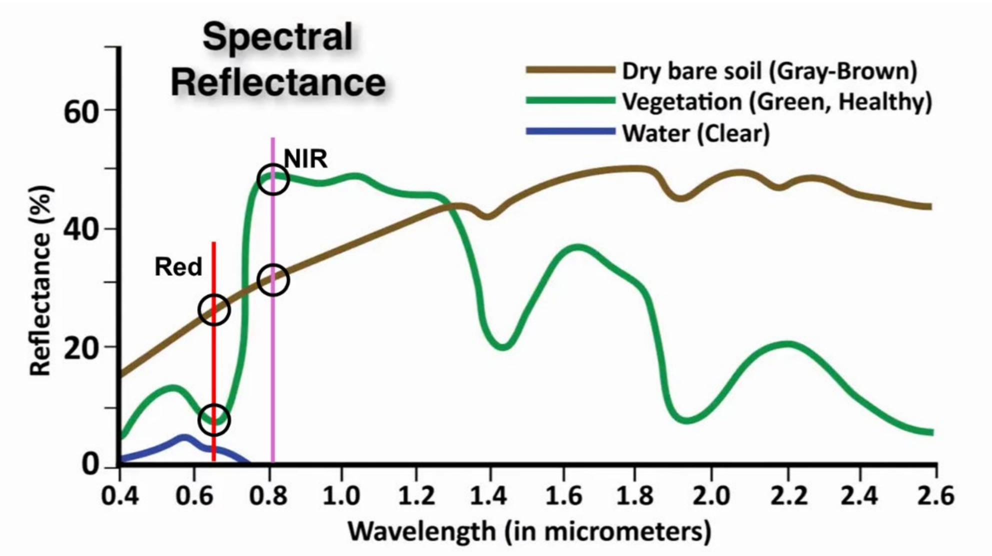

Fig. R3 The typical spectral reflectance curves of soil, vegetation, and water. (adapted from (Siegmund and Menz, 2005).

This study used the nadir reflectance product (MCD43A4) corresponding to local solar noon to calculate NDVI; therefore, the solar-viewing geometry of NDVI is consistent. The consistent geometry and the normalization characteristic of NDVI diminish the angular variation but ensure consistency. In addition, NDVI negatively correlates to

LIA as stated above, and contains vegetation type and vegetation cover information, which was combined with BRDF and other features to improve MLA mapping.

GEDI LiDAR is indeed a powerful sensor to detect canopy structures, such as tree height, fractional vegetation cover, and LAI profile (Tang et al., 2016; Dubayah et al., 2020). Estimating MLA from GEDI LiDAR is an interesting and challenging topic, and no related studies have been reported due to the difficulty in decoupling MLA from LAI by the GEDI LiDAR waveform data. In the GEDI LAI retrieval algorithm, MLA is a key input and is assumed as constant (57.3°) due to the lack of MLA information (Tang et al., 2016). The MLA map generated in this study can be used to improve this issue.

3). In Table 1, MCD12Q1 and MCD43A4 are listed as Collection 6, while other MODIS products are Collection 6.1. The discrepancy in MODIS versions needs clarification. Furthermore, MODIS BRDF (MCD43) and surface reflectance products can be contaminated by clouds, especially in tropical regions. The manuscript should explicitly describe how these cloud gaps or low-quality observations were handled to ensure their usage in the subsequent modeling.

The MCD12Q1 C6 and MCD43A4 V6 were employed in this study (Table 1) because the Collection 6.1 versions were unavailable on the Google Earth Engine when conducting the MLA mapping. The official document indicates that only minor reprocessing including calibration change and polarization correction was adopted in the upgrading from Collection 6 to 6.1, while the MCD12Q1 and MCD43A4 algorithms remain unchanged (https://landweb.modaps.eosdis.nasa.gov/data/userguide/MODIS_Land_C61_Changes.pdf). Previous validation studies with ground truth references have demonstrated that the improvement from C6 to C6.1 (aerosol products, land surface temperature products) is very small ($\triangle R^2 < 0.02$), and the accuracy may even decrease (Che et al., 2019; Bilal et al., 2018; Zhao et al., 2024; Huang et al., 2024). MCD12Q1 and MCD43A4 C6 were already used by numerous studies (Giglio et al., 2018; Rodrigues et al., 2019; Zeng et al., 2022; Wang et al., 2018). The multi-year aggregation of these products (Table 2) further reduces the impact of the slight difference between these two versions. Therefore, we think that the version difference will not make a significant impact on MLA mapping. Following the comment, We have added these explanations to Section 2.2.1.

> *We used MCD43A1 C6.1 and MCD12Q1 and MCD43A4 C6 for MLA mapping as these data were available on GEE when this study was conducted. Only minor*

calibration changes and polarization correction were adopted in the upgrading from Collection 6 to 6.1, while the MCD12Q1 and MCD43A4 algorithms remain the same (https://landweb.modaps.eosdis.nasa.gov/data/userguide/MODIS_Land_C61_Changes.pdf). In addition, the multi-year aggregation of these products (Table 2) further mitigates the version impact.

We agree with the referee that MODIS BRDF (MCD43A1) and surface reflectance products (MCD43A4) used for MLA mapping (section 2.3.2) may be contaminated by clouds, especially in tropical regions. MODIS BRDF is produced daily using multi-date, cloud-cleared, atmospherically corrected input data measured over neighboring 16-day periods (https://lpdaac.usgs.gov/products/mcd43a1v061/). When there is not enough observation to derive BRDF robustly because of the cloud contamination, a backup algorithm is employed which uses prior BRDF shapes and adjusts them with limited observations. This study used all observations including low-quality backup BRDF inversions. This practice has been adopted in global clumping index mapping with BRDF products and a corresponding quality indicator has been provided (Wei et al., 2019). Because we utilized the multi-year aggregation (10%, 33%, 50%, 67%, 90% quantiles, and standard deviation, Table 2) of BRDF and surface reflectance in the MLA mapping, the influence induced by low-quality inversions can be partly mitigated (Sulla-Menashe et al., 2019). In response to the comment, we have added these explanations to section 2.3.2.

This study used all MODIS BRDF and spectral reflectance data including low-quality ones that may be contaminated by clouds. The multi-year aggregation (Table 2) can partly mitigate the influence induced by low-quality observations (Sulla-Menashe et al., 2019).

In addition, we have added a quality layer regarding the proportion of high-quality BRDF inversions (see reply to comment #4 below).

4). As the first global MLA product, it would be valuable to include an uncertainty assessment layer. This might account for the uncertainties stemming from (1) the upscaling approach, (2) the machine learning model, and (3) data inputs. Presenting an explicit uncertainty layer would markedly improve the credibility and potential applications of this novel dataset.

We thank the referee for the recognition and excellent suggestion! We have reconsidered the uncertainty sources of MLA mapping, including the upscaling approach, data inputs, and machine learning model. The upscaling approach mainly influences the uncertainty of training samples which is difficult to quantify for each pixel. The rigorous sample screening after the upscaling process ensures the sample representativeness (section 2.3.1) and reduces the uncertainty raised by the upscaling process. The random forest algorithm is also robust to the remained sample uncertainty as mentioned above.

Regarding model inputs, BRDF and BRDF-adjusted surface reflectance products are important for MLA mapping (Fig. 6), and the same qualitative quality layer indicating whether full BRDF inversions are provided for these products. This study used all observations including low-quality backup BRDF inversions as stated above. Therefore, we have added a quantitative quality layer to represent the proportion of high-quality BRDF inversions for each pixel.

In terms of the prediction model, the machine learning model is typically regarded as a black box, and evaluating the uncertainty for the random forest algorithm is difficult under the current technological background. The random forest algorithm is accurate enough for the predictions fall into the feature space ranges of training samples. For the predictions out of the range of sample features, extrapolation is necessary and the uncertainty is higher. Therefore, the prediction model quality was expressed qualitatively for each pixel considering whether the MLA is predicted by extrapolating beyond the range of the training samples.

Fig. R4 shows the quality layers regarding inputs and prediction model. The global mean proportion of high-quality BRDF inputs is 68.03%. Northern South America and Central Africa have a low proportion of high-quality inputs (20%) due to cloud contamination (Fig. R4 (a)). Considering the large number of observations for each pixel (7904 from 2001 to 2022), this percentage (20%) of high-quality observations is sufficient to map MLA. In addition, 80.39% of the global MLA map was derived within the feature ranges of training samples, and the rest 19.61% were mainly located in high-latitude regions and Africa. For the latter areas, the MLA map was predicted with extrapolation and caution should be taken when using the map (Fig. R4 (b)).

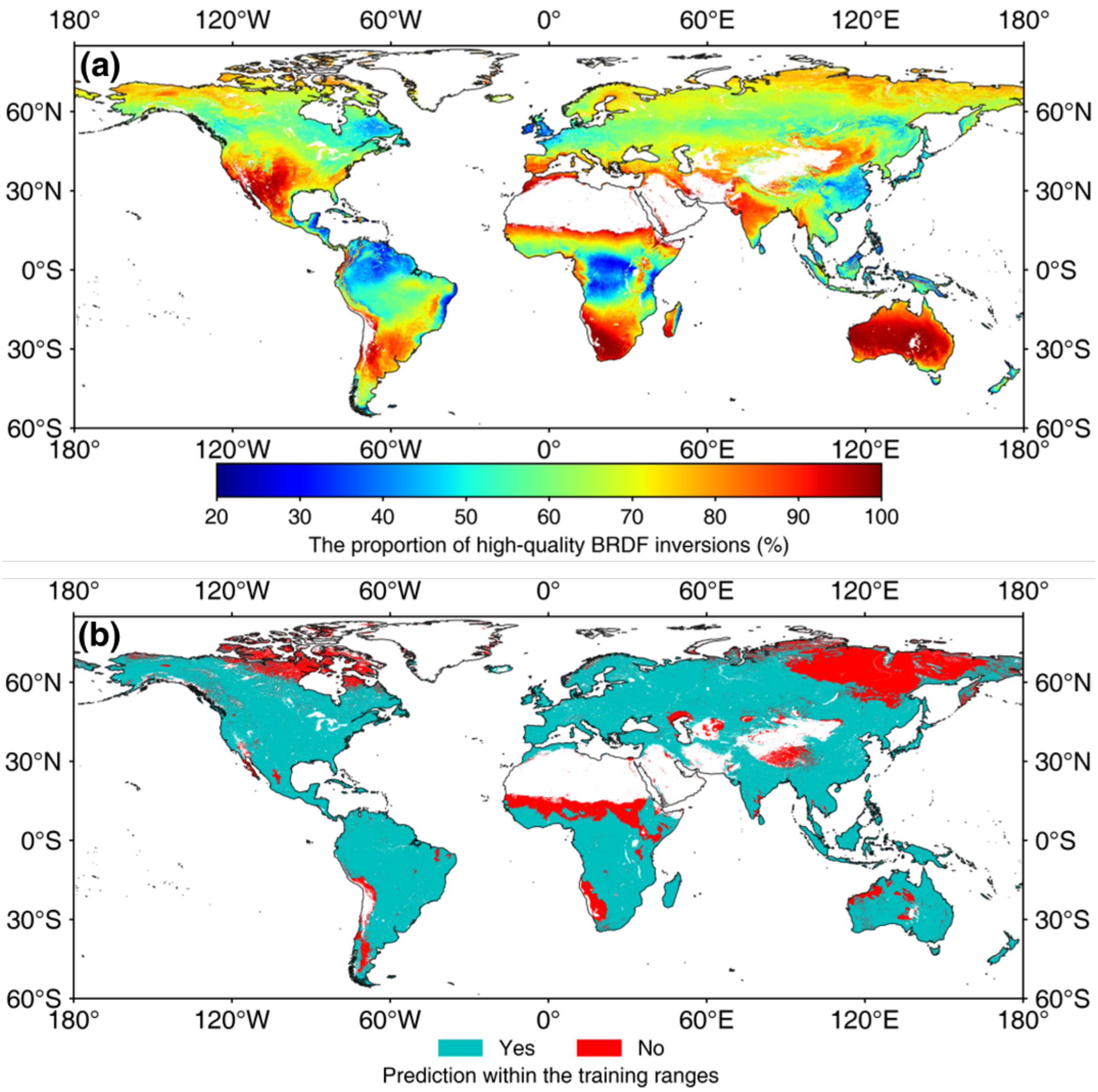

Fig. R4 Global distributions of quality indicators. (a) and (b) denote the proportion of high-quality BRDF inversions, and whether the prediction is within the ranges of training samples, respectively.

In response to the comment, we have added the contents regarding quality layers to Sections 2.3.2 and 3.3. In addition, the data products released on Zenodo have been updated (https://doi.org/10.5281/zenodo.12739662).

Section 2.3.2

Two quality layers were added to represent the quality of input data and the prediction model. The input data quality was denoted by the proportion of high-quality BRDF inversions for each pixel. The prediction model quality was represented qualitatively for each pixel considering whether the MLA was predicted by extrapolating beyond the range of the training samples. The random *forest model is typically regarded as a black-box and its uncertainty is difficult to quantify in the present study.*

Section 3.3

Fig. 12 demonstrates the global distributions of the MLA quality indicators. The global mean proportion of high-quality BRDF inputs is 68.03%. Northern South America and Central Africa have a low proportion of high-quality inputs (20%) because of cloud contamination (Fig. 12 (a)). Considering the large number of observations for each pixel (7904 from 2001 to 2022), this percentage (20%) of high-quality observations is sufficient to map MLA. In addition, 80.39% of the global MLA map was derived within the feature ranges of training samples, and the rest 19.61% were mainly located in high-latitude regions and Africa. For the latter areas, the MLA map was predicted with extrapolation and caution should be taken when using the map (Fig. 12 (b)).

Anonymous referee #3

Thanks to the authors for the meticulous revisions. My key concerns have been addressed in this revised manuscript. I have one new suggestion. Although the authors have conducted experiments to prove that the nonlinear relationship between LAI (Leaf Area Index) and EVI (Enhanced Vegetation Index) has little impact on the results, I suggest that the reasons for the nonlinearity of LAI-EVI, especially the saturation phenomenon, should be elaborated in the text. In addition, why not use other vegetation indices such as NDVI (Normalized Difference Vegetation Index)? Since many papers on the error propagation of vegetation indices, the evaluation of saturation phenomena, and the relationships between vegetation indices and LAI and LCC (Leaf Chlorophyll Content) have been published recently, it is recommended that the author explain why EVI was chosen by citing such papers. Meanwhile, I suggest that the author incorporate more of the responses to the reviewers into the main body of the paper.

We thank the referee for the recognition and suggestion. The slight nonlinearity between LAI and EVI2 is induced by the saturation effect at medium and high LAI conditions where the reflectance in near-infrared and red wavelength is stable (Gao et al., 2023).

In this study, EVI2 was used instead of other vegetation indices. Unlike NDVI, EVI2 is highly resistant to the saturation effect (Gao et al., 2023) and also shows a near-linear correlation with LAI (Dong et al., 2019; Alexandridis et al., 2019).

Following the suggestion, we have added these explanations to Section 2.3.1.

> *Therefore, the 500 m MLA was computed as the weighted average of the enhanced vegetation index (EVI2) assuming a linear relationship between LAI and EVI2 (Dong et al., 2019; Alexandridis et al., 2019). Although previous studies have reported that vegetation index may be nonlinearly correlated to LAI because of the saturation effect at medium and high LAI conditions, EVI2 is highly resistant to the saturation effect (Gao et al., 2023). The errors caused by this slight nonlinearity were further analyzed in Section 4.4.*

In addition, we have incorporated more of the responses to the reviewers into the main body of the paper in the revised version. Specifically, the responses regarding the spatial distribution and representativeness of samples (Section 2.3.1), the importance of biome map in MLA prediction (Section 4.2), the introduction of RS-based vegetation structure parameters as predictive variables (Section 4.4), and the choice of distance threshold (Section 2.3.1) have been further integrated.

Reference

Alexandridis, T. K., Ovakoglou, G., and Clevers, J. G. P. W.: Relationship between MODIS EVI and LAI across time and space, Geocarto International, 35, 1385-1399, 10.1080/10106049.2019.1573928, 2019.

Bilal, M., Nazeer, M., Qiu, Z., Ding, X., and Wei, J.: Global Validation of MODIS C6 and C6.1 Merged Aerosol Products over Diverse Vegetated Surfaces, Remote Sensing, 10, 10.3390/rs10030475, 2018.

Che, H., Yang, L., Liu, C., Xia, X., Wang, Y., Wang, H., Wang, H., Lu, X., and Zhang, X.: Long-term validation of MODIS C6 and C6.1 Dark Target aerosol products over China using CARSNET and AERONET, Chemosphere, 236, 124268, 10.1016/j.chemosphere.2019.06.238, 2019.

Chianucci, F., Pisek, J., Raabe, K., Marchino, L., Ferrara, C., and Corona, P.: A dataset of leaf inclination angles for temperate and boreal broadleaf woody species, Annals of Forest Science, 75, 50-50, 10.1007/s13595-018-0730-x, 2018.

de Wit, C. T.: Photosynthesis of leaf canopies, Pudoc, 1965.

Dong, T., Liu, J., Shang, J., Qian, B., Ma, B., Kovacs, J. M., Walters, D., Jiao, X., Geng, X., and Shi, Y.: Assessment of red-edge vegetation indices for crop leaf area index estimation, Remote Sens. Environ., 222, 133-143, 10.1016/j.rse.2018.12.032, 2019.

Dubayah, R., Blair, J. B., Goetz, S., Fatoyinbo, L., Hansen, M., Healey, S., Hofton, M., Hurtt, G., Kellner, J., Luthcke, S., Armston, J., Tang, H., Duncanson, L., Hancock, S., Jantz, P., Marselis, S., Patterson, P. L., Qi, W., and Silva, C.: The Global Ecosystem Dynamics Investigation: High-resolution laser ranging of the Earth’s forests and topography, Science of Remote Sensing, 1, 10.1016/j.srs.2020.100002, 2020.

Fang, H., Baret, F., Plummer, S., and Schaepman-Strub, G.: An Overview of Global Leaf Area Index (LAI): Methods, Products, Validation, and Applications, Rev. Geophys., 57, 739-799, 10.1029/2018rg000608, 2019.

Gao, S., Zhong, R., Yan, K., Ma, X., Chen, X., Pu, J., Gao, S., Qi, J., Yin, G., and Myneni, R. B.: Evaluating the saturation effect of vegetation indices in forests using 3D radiative transfer simulations and satellite observations, Remote Sens. Environ., 295, 10.1016/j.rse.2023.113665, 2023.

Giglio, L., Boschetti, L., Roy, D. P., Humber, M. L., and Justice, C. O.: The Collection 6 MODIS burned area mapping algorithm and product, Remote Sens. Environ., 217, 72-85, 2018.

Huang, G., Su, X., Wang, L., Wang, Y., Cao, M., Wang, L., Ma, X., Zhao, Y., and Yang, L.: Evaluation and analysis of long-term MODIS MAIAC aerosol products in China, Sci. Total Environ., 948, 174983, 10.1016/j.scitotenv.2024.174983, 2024.

Moreno-Martínez, Á., Camps-Valls, G., Kattge, J., Robinson, N., Reichstein, M., van Bodegom, P., Kramer, K., Cornelissen, J. H. C., Reich, P., Bahn, M., Niinemets, Ü., Peñuelas, J., Craine, J. M., Cerabolini, B. E. L., Minden, V., Laughlin, D. C., Sack, L., Allred, B., Baraloto, C., Byun, C., Soudzilovskaia, N. A., and Running, S. W.: A methodology to derive global maps of leaf traits using remote sensing and climate data, Remote Sens. Environ., 218, 69-88, 10.1016/j.rse.2018.09.006, 2018.

Pisek, J., Ryu, Y., and Alikas, K.: Estimating leaf inclination and G-function from leveled digital camera photography in broadleaf canopies, Trees, 25, 919-924, 10.1007/s00468-011-0566-6, 2011.

Rodrigues, J. A., Libonati, R., Pereira, A. A., Nogueira, J. M., Santos, F. L., Peres, L. F., Santa Rosa, A., Schroeder, W., Pereira, J. M., and Giglio, L.: How well do global burned area products represent fire patterns in the Brazilian Savannas biome? An accuracy assessment of the MCD64 collections, International Journal of Applied Earth Observation and Geoinformation, 78, 318-331, 2019.

Ryu, Y., Sonnentag, O., Nilson, T., Vargas, R., Kobayashi, H., Wenk, R., and Baldocchi, D. D.: How to quantify tree leaf area index in an open savanna ecosystem: A multi-instrument and multi-model approach, Agricultural and Forest Meteorology, 150, 63-76, 10.1016/j.agrformet.2009.08.007, 2010.

Siegmund, A. and Menz, G.: Fernes nah gebracht–Satelliten-und Luftbildeinsatz zur Analyse von Umweltveränderungen im Geographieunterricht, Geographie und Schule, 154, 2-10, 2005.

Sulla-Menashe, D., Gray, J. M., Abercrombie, S. P., and Friedl, M. A.: Hierarchical mapping of annual global land cover 2001 to present: The MODIS Collection 6 Land Cover product, Remote Sens. Environ., 222, 183-194, 10.1016/j.rse.2018.12.013, 2019.

Svetnik, V., Liaw, A., Tong, C., Culberson, J. C., Sheridan, R. P., and Feuston, B. P.: Random forest: a classification and regression tool for compound classification and QSAR modeling, Journal of chemical information and computer sciences, 43, 1947-1958, 2003.

Tang, H., Ganguly, S., Zhang, G., Hofton, M. A., Nelson, R. F., and Dubayah, R.: Characterizing leaf area index (LAI) and vertical foliage profile (VFP) over the United States, Biogeosciences, 13, 239-252, 10.5194/bg-13-239-2016, 2016.

Wang, Z., Schaaf, C. B., Sun, Q., Shuai, Y., and Román, M. O.: Capturing rapid land surface dynamics with Collection V006 MODIS BRDF/NBAR/Albedo (MCD43) products, Remote Sens. Environ., 207, 50-64, 2018.

Wei, S., Fang, H., Schaaf, C. B., He, L., and Chen, J. M.: Global 500 m clumping index product derived from MODIS BRDF data (2001–2017), Remote Sens. Environ., 232, 111296, https://doi.org/10.1016/j.rse.2019.111296, 2019.

Yan, G., Jiang, H., Luo, J., Mu, X., Li, F., Qi, J., Hu, R., Xie, D., and Zhou, G.: Quantitative Evaluation of Leaf Inclination Angle Distribution on Leaf Area Index Retrieval of Coniferous Canopies, Journal of Remote Sensing, 2021, 1-15, 10.34133/2021/2708904, 2021.

Zeng, Y., Hao, D., Huete, A., Dechant, B., Berry, J., Chen, J. M., Joiner, J., Frankenberg, C., Bond-Lamberty, B., and Ryu, Y.: Optical vegetation indices for monitoring terrestrial ecosystems globally, Nature Reviews Earth & Environment, 3, 477-493, 2022.

Zhao, R., Yu, W., Deng, X., Huang, Y., Yang, W., and Zhou, W.: Analysis of Land Surface Performance Differences and Uncertainty in Multiple Versions of MODIS LST Products, Remote Sensing, 16, 10.3390/rs16224255, 2024.

Zou, X., Mõttus, M., Tammeorg, P., Torres, C. L., Takala, T., Pisek, J., Mäkelä, P., Stoddard, F. L., and Pellikka, P.: Photographic measurement of leaf angles in field crops, Agricultural and Forest Meteorology, 184, 137-146, 10.1016/j.agrformet.2013.09.010, 2014.